

Role of free volume in strain softening of as-cast and annealed bulk metallic glass

Byung-Gil Yoo

Division of Materials Science and Engineering, Hanyang University, Seoul 133-791, Korea

Kyoung-Won Park and Jae-Chul Lee

Department of Materials Science and Engineering, Korea University, Seoul 136-701, Korea

U. Ramamurty

Department of Materials Engineering, Indian Institute of Science, Bangalore 560012, India

Jae-il Jang^{a)}

Division of Materials Science and Engineering, Hanyang University, Seoul 133-791, Korea

(Received 22 September 2008; accepted 24 November 2008)

Plasticity in amorphous alloys is associated with strain softening, induced by the creation of additional free volume during deformation. In this paper, the role of free volume, which was a priori in the material, on work softening was investigated. For this, an as-cast Zr-based bulk metallic glass (BMG) was systematically annealed below its glass transition temperature, so as to reduce the free volume content. The bonded-interface indentation technique is used to generate extensively deformed and well defined plastic zones. Nanoindentation was utilized to estimate the hardness of the deformed as well as undeformed regions. The results show that the structural relaxation annealing enhances the hardness and that both the subsurface shear band number density and the plastic zone size decrease with annealing time. The serrations in the nanoindentation load-displacement curves become smoother with structural relaxation. Regardless of the annealing condition, the nanohardness of the deformed regions is $\sim 12\text{--}15\%$ lower, implying that the prior free volume only changes the yield stress (or hardness) but not the relative flow stress (or the extent of strain softening). Statistical distributions of the nanohardness obtained from deformed and undeformed regions have no overlap, suggesting that shear band number density has no influence on the plastic characteristics of the deformed region.

I. INTRODUCTION

Plastic deformation in metallic glasses is distinctly different from that in crystalline metals. The fundamental carriers of plasticity in amorphous alloys are shear transformation zones (STZs), which occur through cooperative shear displacements of clusters of atoms in response to the applied load.¹ This deformation mode has two key attributes. (i) The matrix surrounding the STZ has to accommodate the dilation associated with the STZ operation. This results in pressure sensitivity of plastic flow, which in turn has many important consequences in terms of mechanical properties.^{2–4} (ii) STZs occur, preferentially, in those regions that are readily amenable to plasticity by virtue of having lower than average atomic density. For amorphous materials, there are a number of different ways of describing this intrinsic state variable of atomic density, free volume being the most popular

one.^{5,6} “Liquid-like regions,”⁷ local shear modulus,⁸ fictive temperature,⁹ and atomic packing density¹⁰ are other descriptors.

Considerable attention is paid, in the recent literature, to understanding the influence of free volume on plastic deformation of amorphous alloys. The driving force for such studies is the development of a detailed understanding of the origins of ductility and toughness in bulk metallic glasses (BMGs), a new class of structural materials with a unique and attractive set of properties. One way to vary the free volume systematically is to induce structural relaxation in the metallic glasses through annealing heat treatments below the glass transition temperature, T_g .^{11–15} Structural relaxation, which does not lead to crystallization, reduces the free volume by annihilation and such free volume reduction is known to have pronounced influence on the mechanical behavior of BMGs. These include severe embrittlement, change in the ductile-to-brittle transition temperature, fatigue characteristics, and so on, of the as-cast material.^{16–20} In contrast, experiments on BMG samples that were

^{a)}Address all correspondence to this author.

e-mail: jijang@hanyang.ac.kr

DOI: 10.1557/JMR.2009.0167

already deformed extensively by mechanical processes such as rolling, show that post-deformation annealing enhances ductility.²¹

In addition to the free volume that is present in a given amorphous alloy, the free volume model of Spaepen⁵ suggests that a considerable amount of excess free volume can be produced during plastic deformation. The free volume thus generated causes strain softening of the plastic flow, which in turn leads to localization of flow into narrow regions known as shear bands.^{1,22,23} The instrumented indentation technique, especially nanoindentation, is widely used for investigating the shear band plasticity in metallic glasses, which manifests as serrations in indentation load-displacement (P - h) curves. Examination of these serrations allows for detailed studies on rate and temperature effects on plasticity.^{1,24} If the tests are performed under load control, discrete displacement jumps or pop-ins are seen in the loading part of the P - h curve, whereas the displacement control tests show sudden load drops.

Recently, Bhowmick et al.²⁵ have used the bonded-interface technique to generate a well defined plastic flow zone underneath the indenter, which in turn was probed with nanoindentation to demonstrate that it is relatively softer than the undeformed material far away from the indenter tip. In this paper, we extend this work to examine the following issues related to plasticity in BMGs. While it is now well established that plastic flow causes softening of the BMG, the role played by the free volume content at the start is not known. For example, “will all amorphous alloys strain soften, irrespective of the prior free volume content?” is a question that has not been answered yet. A related question is, “if all amorphous alloys strain soften, to what extent do they strain soften, that is, will a BMG with higher amount of free volume at the start of the plastic deformation strain soften less than an alloy with lower amount of free volume?” Prior work by Ramamurty and coworkers^{17,26} has shown that reducing the free volume content decreases the shear band number density in the deformed zones. Consequently, “does the number density of shear bands determine the extent of softening?” is also an important question to examine. Here we seek to address these issues, which have important bearing for better understanding of plasticity in BMGs, through systematic experiments on annealed BMG samples.

II. EXPERIMENTS

The bulk metallic glass that examined in this work is a Zr-based BMG, $Zr_{52.5}Cu_{17.9}Ni_{14.6}Al_{10}Ti_5$ (commercially designated as Vit 105), which was obtained in the form of a rod having a diameter of ~ 7 mm and a length of ~ 70 mm. The sample, of which the glass-transition temperature (T_g) and the onset temperature of the

crystallization (T_x) are ~ 673 and ~ 720 K, respectively, was annealed at 630 K ($0.93T_g$) for two different times (20 and 90 min). To examine the possibility of inducement of crystallization during annealing, x-ray diffraction (XRD) of the as-cast and annealed specimens was performed using D/MAX-2500 (Rigaku-Denki, Japan). To estimate the free volume change during annealing, differential scanning calorimetry (DSC) of all the specimens was performed using a Perkin-Elmer DSC-7 (PerkinElmer Inc., Waltham, MA) in a purified Ar atmosphere at a fixed heating rate of 20 K/min.

The interface-bonded specimens for macroscopic spherical indentation were prepared by cutting the rod first into two halves and then polishing them to a mirror finish prior to bonding them using a high-strength adhesive (Loctite, Henkel Ireland Ltd., Ireland). Subsequently, the top surface of the bonded specimen was polished to a mirror finish. On the bonded interface, spherical indentations were performed using an instrumented indentation equipment, AIS-2100 (Frontics Inc., Seoul, Korea), with a WC ball indenter having a radius of 500 μm . The applied indentation loads were 98 N and 196 N, both with a fixed loading rate of 5 $\mu\text{m/s}$. After this macroscopic spherical indentation, the bonded interface was opened by dissolving the adhesive in acetone, and then the subsurface deformation morphology was examined through optical microscopy. It should be noted that the finite width of the complaint bond in the bonded interface technique allows for the relaxation of the plastic constraint (that is otherwise present underneath the indenter). This, in turn, allows for plastic flow into the interface. For example, semicircular shear bands might be the result of the constraint release by the interface. Although the interface-bonded sample cannot generate exactly the same fields of stress and strain during indentation as those in a bulk sample without an interface, it is generally believed that one can gain insight for better understanding the plasticity underneath the indenter by observing the subsurface deformation morphology of the samples. The soft adhesive effect might be avoided if the mechanical clamping method is applied for bonding the interface instead of using adhesive. However, clamping the sample in a vice can induce a large additional stress in the specimen.

Subsequent to the characterization of the subsurface plastic zone, it was gently polished using alumina particle of 0.3 μm or diamond paste of 0.5 μm to make it flat for nanoindentation. To evaluate the hardness distribution within the subsurface deformation region, a series of nanoindentation experiments were performed on the polished surface using a Nanoindenter-XP (Nano Instruments, Oak Ridge, TN) with two three-sided pyramidal indenters having a different centerline-to-face angle; 65.3° (Berkovich indenter) and 35.3° (cube-corner indenter). The nanoindentation hardness (often called

nanohardness) was measured according to the Oliver-Pharr method,^{27,28} with the Berkovich indenter at a maximum indentation load of 50 mN and the strain rate of 0.5 s⁻¹. To avoid possible artifacts, thermal drift was maintained below 0.05 nm/s. After nanoindentation, the profiles of the indented surfaces were examined by atomic force microscopy (AFM) XE-100 (Park Systems, Suwon, Korea).

III. RESULTS

A. Structural characterization

Figure 1 shows the XRD scans of the as-cast and annealed samples. Because the annealing temperature, 630 K, is below the T_g of the BMG, no perceptible crystalline peaks could be detected in the XRD spectra, suggesting that even the 90-min-annealed sample was not crystallized but only structurally relaxed.

To examine the change in structural characteristics in more detail, DSC analysis was performed in a manner similar to that reported in literature.^{14,16,17} These studies show that the exothermic heat flow at the glass transition (ΔH) is directly associated with the degree of annihilation of excess free volume. Slipenyuk and Eckert¹⁴ experimentally verified that there is a linear relation between ΔH and the reduced amount of free volume (Δv_f) during structural relaxation of a Zr-based BMG. Figure 2(a) shows the DSC thermograms recorded from the as-cast and annealed samples. The inset of the figure (showing a magnified view of the thermograms below T_g) reveals that the amount of exothermic heat flow decreases as the annealing time increases. Estimated amounts of ΔH , calculated by integrating the exothermic heat flow near the glass transition, are summarized as a function of annealing time in Fig. 2(b). It shows that

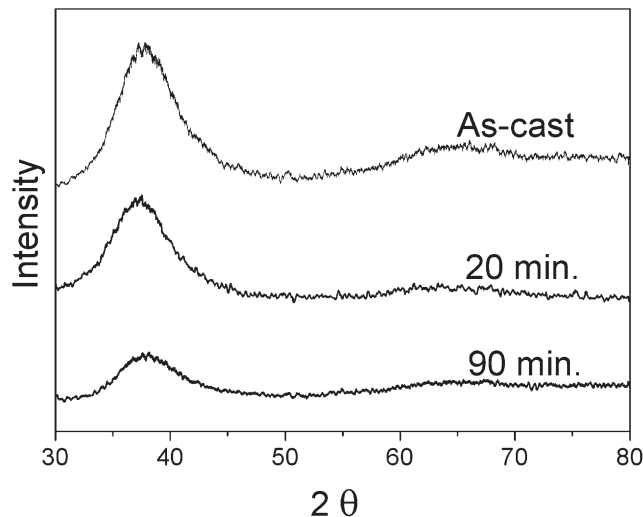


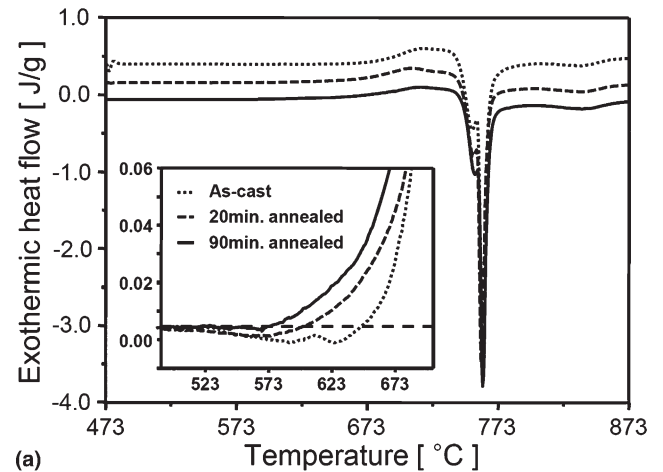
FIG. 1. X-ray diffraction patterns of the as-cast and annealed specimens.

annealing reduces the ΔH , and in turn the amount of free volume, significantly.

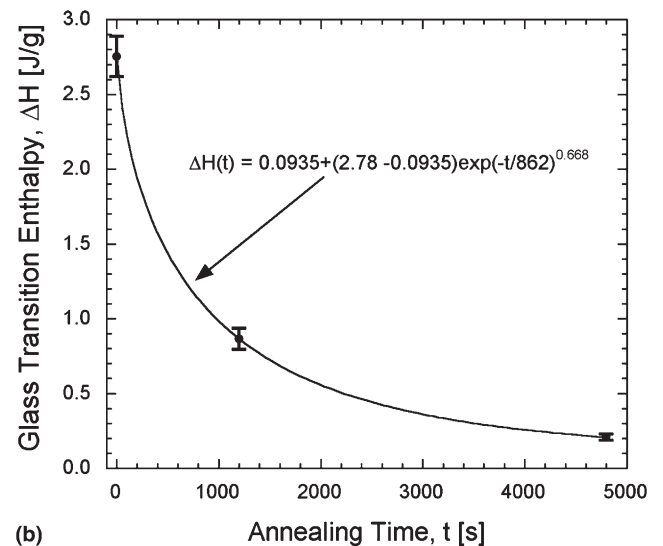
Structural relaxation in glasses can involve the simultaneous operation of many processes, each associated with a characteristic timescale. The stretched exponential function is a frequently used empirical relation to describe the relaxation rates associated with any physical property. In the context of the enthalpy change at the glass transition, it can be written as^{11,17,29}

$$\Delta H(t) = \Delta H(\infty) + [\Delta H(0) - \Delta H(\infty)] \exp(-t/\tau)^\beta, \quad (1)$$

where $\Delta H(t)$, $\Delta H(0)$, and $\Delta H(\infty)$ are the values of ΔH at times t , 0, and ∞ , respectively, τ is the average relaxation time, and β is the stretched exponent. β is independent of the annealing temperature in principle and can



(a)



(b)

FIG. 2. DSC analysis of structural change; (a) DSC scan of the as-cast and annealed samples with inset showing subtle calorimetric difference; (b) variation in the exothermic heat flow as a function of annealing time.

vary between 0 and 1. $\beta \approx 1$ implies that the system is a strong glass former whereas $\beta < 0.5$ implies that the glass is fragile.^{30,31} A regression fit of Eq. (1) through the data in Fig. 2(b), with $\Delta H(0)$, $\Delta H(\infty)$, τ , and β as variable parameters, yields values of 0.0935 J/g, 2.78 J/g, 862 s, and 0.668, respectively, with a goodness of fit $R^2 = 1$, suggesting excellent correlation. The latter two are consistent with the literature values.³¹

B. Subsurface deformation morphology

Figure 3 shows the optical micrographs of the deformation region underneath the spherical indentation impressions. In the as-cast as well as the annealed samples, the size of the plastic deformation zone, which has multiple shear bands, increases with the maximum load of spherical indentation, as expected. It is instructive

to note that, in Fig. 3(e), the initial formation (or nucleation) of shear bands occurs not just beneath the indented surface but at a distance from the surface. This is because the maximum shear stress during spherical indentation is obtained at a distance of about 0.45 times the contact radius (a) below the specimen surface.³²

Importantly, Fig. 3 illustrates the sub- T_g annealing effect on the size of the deformed zone and the shear band number density at a given load, both of which decrease with increasing annealing time. For example, the variation in plastic zone size at a 196 N load (which was determined as the radial distance of the outermost shear band as shown in the inset of Fig. 4) as a function of the annealing time is shown in Fig. 4, exhibiting the decrease in the plastic zone size with the annealing time. This indicates that the indentation-induced plasticity is limited in the annealed samples compared to that in the

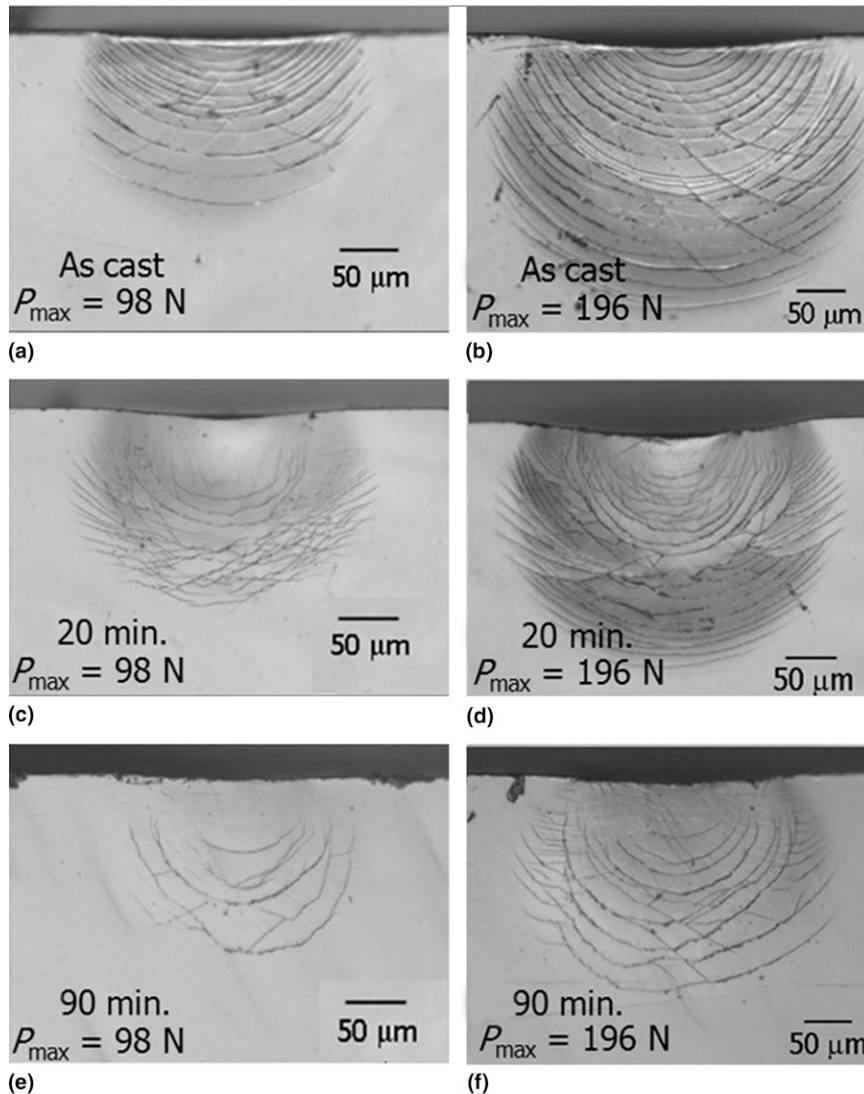


FIG. 3. Load-displacement (P - h) curves recorded during macroscopic spherical indentations on the bonded-interface at the maximum loads of 98 N and 196 N.

as-cast sample, which is consistent with the results of Ramamurty and coworkers.^{17,26} The shear bands in the as-cast sample [Figs. 3(a) and 3(b)] can be broadly categorized into two types; semicircular and radial shear bands. For the as-cast sample, only semicircular shear bands were observed underneath the indentation made at 98 N [Fig. 3(a)]. At 196 N, a few secondary radial shear bands appear in addition to the semicircular shear bands [Fig. 3(b)]. For the annealed samples, however, the secondary radial bands are rarely observed within the subsurface deformation region. This relatively limited plasticity in the annealed samples is a consequence of the reduction in free volume due to structural relaxation; as macroscopic plasticity in BMG is controlled by shear banding behavior, the decreased probability of shear band nucleation due to the reduction in free volume can result in the dramatic decay in shear band activity and thus plastic deformation.^{16,17,26}

The spacing of semicircular shear bands was measured along the centerline from the indented surface [see the inset of Fig. 5(a)], and plotted as a function of the distance from the tip in Fig. 5(a) and of the annealing

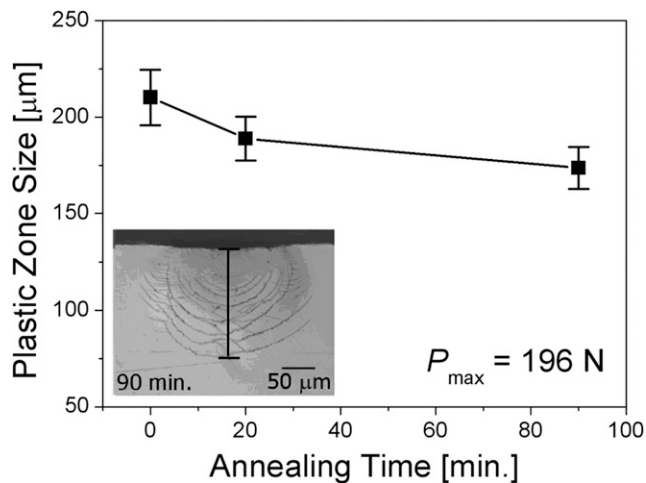


FIG. 4. Change in plastic zone size at 196 N load (which was determined as the radial distance of the outermost shear band) with the annealing time.

time in Fig. 5(b). Note that the data in Fig. 5(b) were taken from the regime for the distance of 50–150 μm in Fig. 5(a). For the as-cast sample, the interband spacing is in the range of 5–20 μm , similar to the values for a Zr-Cu-Ti-Ni-Be BMG previously reported.²⁵ Further, it is almost independent of the maximum load applied, despite statistical fluctuations. The spacing is much higher in the annealed samples and decreases with increasing load from 98 N to 196 N. This implies that, for the annealed samples, as the plastic strain increases, a new shear band nucleates between the preexisting shear bands and hence the line density of shear bands increases. Conversely, in the case of the as-cast sample, there is no dramatic change in the shear band density with increasing indentation strain.

Another clue for relatively limited plasticity in the annealed sample vis-à-vis the as-cast sample can be found in Fig. 6, which shows the P - h curves of nano-indentation made with a cube-corner indenter. The annealed sample exhibits a smaller indentation depth at any given indentation load than the as-cast sample. This observation implies a significant increase in hardness due to structural relaxation. This observation is consistent with the previous results on the same material by Dmowski et al.¹⁵ who demonstrated a rapid increase in micro-hardness after annealing for a short time. The P - h curves show continuous serrations (serial pop-ins) that are associated with shear band nucleation and/or propagation.^{33–38} Using a cube-corner indenter instead of a typical Berkovich indenter is based on the fact that the sharper cube-corner indenter produces much higher stresses and strains than the Berkovich indenter,^{39,40} making it possible to clearly observe serrations.^{41–43} In Fig. 6, the serrated flows seem to strongly depend on the annealing degree. As the annealing time increases, the discrete events gradually weaken. Since the serrations could arise from the inhomogeneous deformation by shear banding activity,^{33–38} this trend is evidence for the decreased shear banding activity in the annealed samples.

Estimating the contribution of the serrations (pop-ins) to the total plastic deformation in the BMG can provide

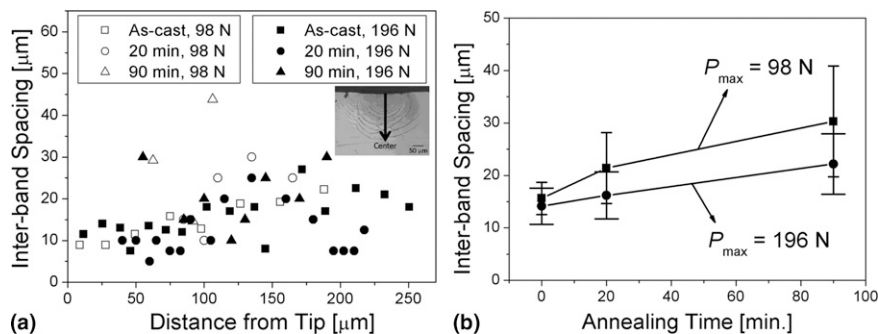


FIG. 5. Variation in the interband spacing as a function of (a) the distance from the tip of the hardness impression, and (b) the annealing time. The data in (b) were taken from the regime for the distance of 50–150 μm in (a).

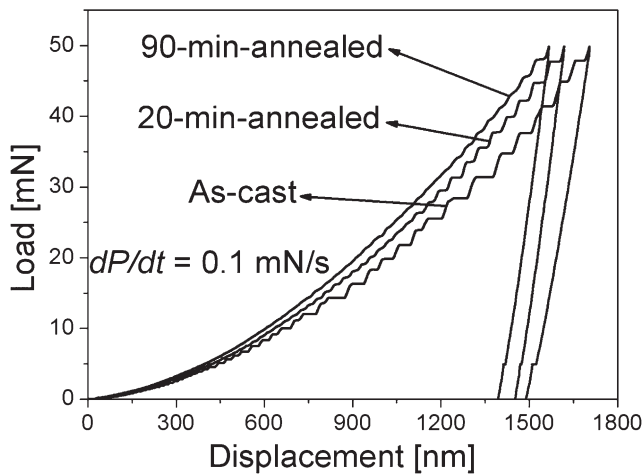


FIG. 6. Typical load-displacement curves obtained from nanoindentation with a cube-corner indenter at a constant loading rate of 0.1 mN/s.

interesting clues for the governing deformation mechanism. For the purpose of this estimation, the following detailed analysis of the discrete displacements was conducted. The total displacement (Δh_{tot}) at a given load during the loading part of nanoindentation can be partitioned, approximately, into three components: (i) displacement associated with the elastic deformation of the solid, Δh_e , (ii) displacement associated with homogeneous plasticity, Δh_{con} , and (iii) displacement associated with discrete plastic deformation, Δh_{dis} . Since the elastic portion of deformation can be expected to be recovered during unloading, Δh_e can be estimated using the unloading part of the P - h curve [see Fig. 7(a)]. The contribution of discrete plasticity to the total plasticity ($\Delta h_{\text{tot}} - \Delta h_e$) can be assessed by examining the discrete plasticity ratio, defined as $\phi = \Delta h_{\text{dis}} / (\Delta h_{\text{con}} + \Delta h_{\text{dis}})$.⁴¹ Note that $\phi = 1$ implies that plasticity is exclusively inhomogeneous (through shear bands), whereas $\phi = 0$ means it is truly homogeneous (as in indentation of metallic polycrystalline materials). Accordingly, as the ratio ϕ increases, the portion of shear-band-mediated plasticity increases and that of STZ-mediated plasticity decreases.

Variation of ϕ with h is plotted in Fig. 7(b) for the as-cast and annealed samples. For the as-cast sample, ϕ appears to be independent of h and only the pop-in size increases with displacement. This implies that the contributions of homogeneous and heterogeneous plasticity (STZ- and shear band-mediated plasticity, respectively) remain approximately constant, with the heterogeneous plasticity contribution being dominant ($\sim 80\%$). For the annealed samples, however, not only the pop-in size but also the discrete plasticity ratio increases with the indentation depth. For h below ~ 1200 nm, the ϕ values of the annealed samples are smaller, whereas above a 1200 nm depth of penetration, both the as-cast and annealed

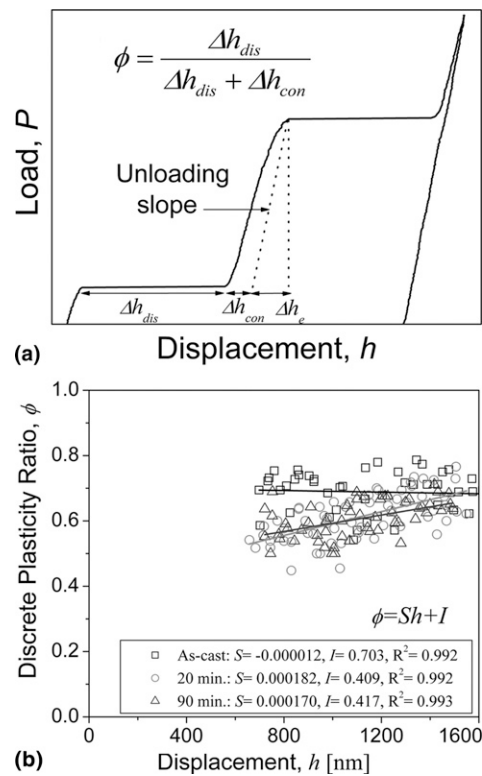


FIG. 7. Calculation of discrete plasticity ratio. (a) How to measure a discrete portion of plastic deformation (Δh_{dis}), a continuous portion of plastic deformation (Δh_{con}), and an elastic portion of deformation (Δh_e). (b) Plot of discrete plasticity ratio, ϕ , versus depth of penetration, h .

samples exhibit similar ϕ values. This implies that STZs and shear bands contribute equally at the initial stages of plasticity in annealed samples, and only at later stages of deformation do shear bands start to dominate the overall plasticity.

C. Hardness of subsurface deformation zone

In order to analyze the mechanical response of the deformed region in Fig. 3, nanoindentation experiments were performed with a Berkovich indenter on the deformed area after gentle polishing. The P - h curves obtained from the undeformed and deformed regions in the as-cast and annealed samples were compared in Fig. 8. For all the samples, there is a clear difference in P - h curves and thus in hardness value. Note that the nanoindentation hardness values were calculated according to the Oliver-Pharr method.^{27,28} Since this method cannot take the pileup (typically observed around the hardness impression of BMGs) into consideration, the hardness value reported here is an overestimate.

The nanohardness data obtained from the deformed region at two different maximum loads (98 N and 196 N) and those obtained from the undeformed regions (i.e., far away from the subsurface shear banded regions)

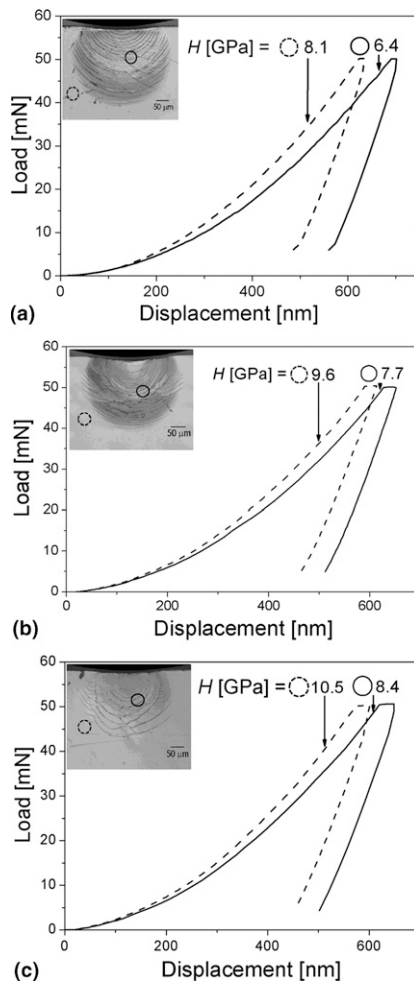


FIG. 8. Representative P - h curves and hardness obtained from the undeformed and the deformed zone underneath the indent; (a) as-cast, (b) 20-min-annealed, and (c) 90-min-annealed specimen.

are plotted as cumulative probability distributions in Fig. 9. Here, Figs. 9(a), 9(b), and 9(c) correspond to the as-cast, 20 min annealed, and 90 min annealed samples, respectively. The cumulative probability of the i th ranked (in ascending order) data point is calculated as $(i - 0.5)/N$ where N is the size of the data set.

The following points are noteworthy. (i) For all the three different conditions, the hardness values of the deformed region are smaller than the corresponding undeformed hardness data. The softening tendency is in good agreement with recent experimental work on the same BMG as used here^{44,45} which report that the hardness of the compressed samples decreases with increasing compressive plastic strain. (ii) The hardness distributions, obtained from the deformed region, are independent of the maximum load applied (98 N or 196 N) and thus are also independent of the indentation strain to generate the plastic zone. (iii) With annealing, the mean hardness of both deformed and

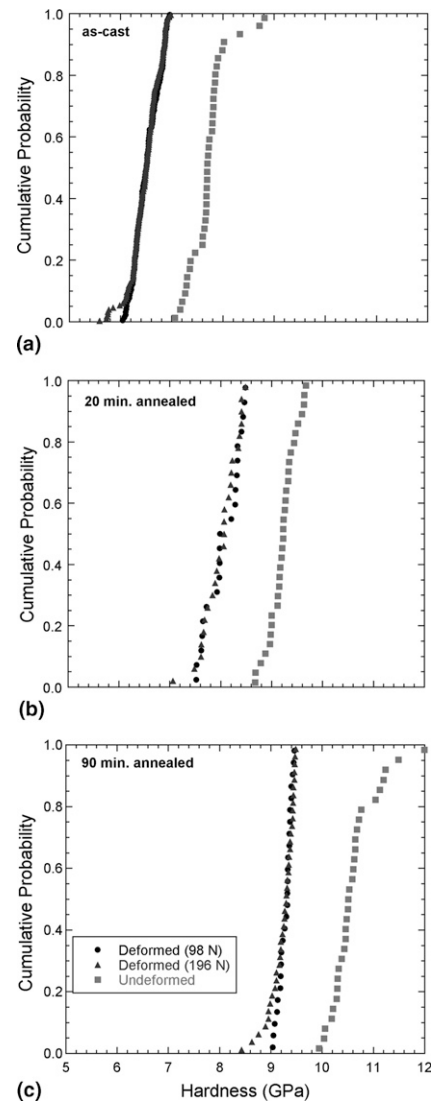


FIG. 9. Cumulative distribution of hardness measured at undeformed and deformed region; (a) as-cast, (b) 20-min-annealed, and (c) 90-min-annealed specimen.

undeformed regions increase. The last point is illustrated in Fig. 10, wherein the average hardness values are plotted as a function of the annealing time. Although it appears that the undeformed and deformed hardness data diverge with annealing time, the relative difference $[(H_{\text{undeformed}} - H_{\text{deformed}})/H_{\text{undeformed}}]$ actually decreases, but only marginally (from $\sim 15.5\%$ to 12.5%).

A key observation that can be made from the hardness distributions of Figs. 9 and 10 is the following. For all the three different material conditions, the highest hardness that is measured from the deformed region is lower than the lowest hardness measured in the undeformed region. This is significant for the following reason. By virtue of shear banding, which is inhomogeneous in nature, the deformed region is inhomogeneous. The area of the nanoindent is $10 \times 10 \mu\text{m}^2$, whereas the interband

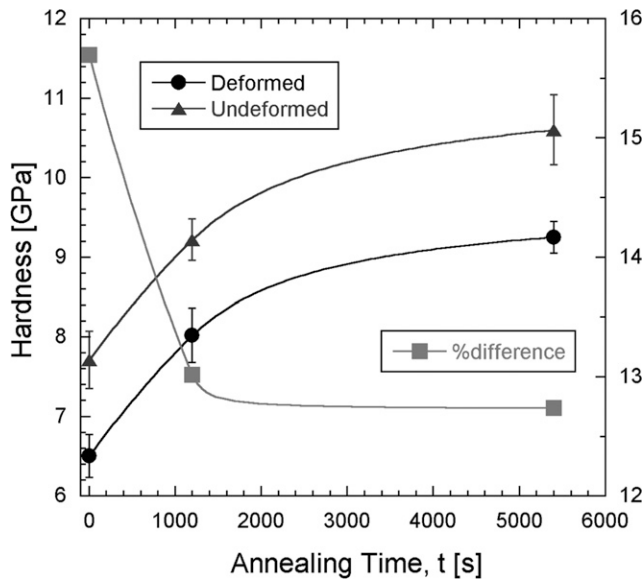


FIG. 10. Change in hardness and its relative difference between deformed and undeformed region as a function of annealing time.

spacing is several tens of μm , especially for the 98 N load case and in the annealed samples. (Note that we could not intentionally make a nanoindentation on the region between the shear bands or on top of a shear band, because the shear band zone was gently polished before nanoindentation.) This being the case, the likelihood of an indent falling in between two shear bands is high. For such indents that do not sample a shear band, the hardness should be at least equal to the lowest hardness measured on an undeformed sample. However, this is not so, with no overlap between the deformed and undeformed distributions. Further, the hardness distributions obtained from the deformed regions are as tight as those obtained from the undeformed regions. (This can be gauged by examining the variance, which is defined as the ratio of the standard deviation to the average value of the distribution. See Table I for data.)

D. Pileup around the nanoindentations

The characteristics of the material pileup around the nanoindentations were evaluated using the AFM to understand the differences in the deformation behavior, if any, of the BMG in different states. At the continuum level, the plasticity in BMGs is volume conserving (for all practical purposes, as the dilatational component is small) and hence can be treated as incompressible. Due to the incompressibility of the material, the material removed from the indented volume can pile up around the indentation.⁴⁶ Figure 11 shows the representative AFM images obtained from the undeformed as well as the deformed regions. In these images, the high height contrast around the impression is due to the material pileup. In the as-cast as well as annealed conditions,

TABLE I. Summary of the nanoindentation test results performed on deformed and undeformed regions of various samples.

Condition	Undeformed region hardness (GPa)	Deformed region hardness (GPa)	Relative difference (%)
As-cast	7.71 ± 0.36 (4.1%)	6.50 ± 0.27 (4.7%)	15.7
20 min annealed	9.22 ± 0.26 (4.2%)	8.02 ± 0.34 (2.8%)	13.0
90 min annealed	10.60 ± 0.44 (2.2%)	9.25 ± 0.20 (4.1%)	12.7

AFM images obtained from the undeformed region exhibit a relatively larger amount of pileup than from the deformed region. Tang et al.,⁴⁷ who made nanoindentations on the free surface around spherical indentation impression, make a similar observation. It is noteworthy that, in Berkovich indentation, the shear bands are mostly captured underneath the indenter and not extended onto the surface, which is different from the case of sharper cube-corner indentation. Thus, the observed pileup after Berkovich indentation is not the shear bands themselves.^{42,48}

The influence of the sub- T_g annealing on the pileup phenomenon is clearly seen in Fig. 11; for both the softened and the undeformed region, a larger amount of pileup is observed in the longer-annealed sample. One might imagine that the reduced amount of free volume plays an important role in the increase in pileup in the annealed sample. Since the structurally relaxed sample has a smaller amount of free volume than the as-cast sample, the reduced free volume can reduce the ability to accommodate plastic deformation induced by nanoindentation. This might result in a higher pileup in the annealed sample than in the as-cast sample.

Based on the above results, it is instructive to clarify that the development of material pileup has an opposite trend on the activity of shear banding behavior, which is often misunderstood. In Berkovich indentation of BMG, the shear bands (which occur mostly underneath the indenter)^{42,48} accommodate the inhomogeneous subsurface deformation. Accordingly, the higher activity of the shear banding (arising from the larger amount of free volume) can lead to a larger plastic deformation and thus a smaller amount of pileup. A comparison of pileup behavior and serrated flow behavior (known to be associated with shear banding) observed in this work supports this hypothesis. From Figs. 6 and 11, it is obvious that less pronounced serrations in the P - h curve (possibly for the lower activity of shear banding) correspond to the larger amount of pileup.

The analogy between the AFM results and the observation by Jiang et al.,²¹ who conducted nanoindentation experiments on a Al-based metallic glass ribbon sample produced by melt-spinning, are noteworthy. They reported that the rolled (i.e., deformed and thus possibly softened) sample shows smaller pileup

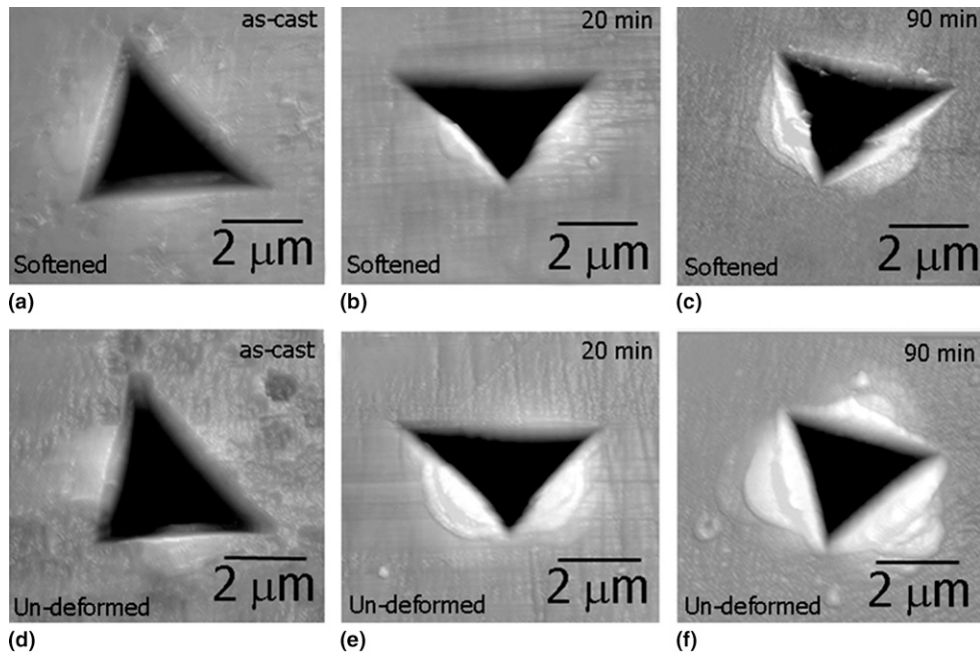


FIG. 11. AFM images of hardness impression produced during Berkovich indentation at $P_{\max} = 50$ mN and $(dh/dt)h^{-1} = 0.5/s$: [(a)–(c)] the softened and the [(d)–(f)] undeformed zone; (a), (d) as-cast sample, (b), (e), the sample annealed for 20 min, and (c), (f) for 90 min.

around the hardness impression than in the as-spun (i.e., undeformed) sample and the rolled/annealed sample exhibits a much higher pileup than in the as-spun sample and the rolled sample. Though they did not provide the AFM analysis for the annealed/rolled sample (which can be analogous to the softened region in the annealed sample in this work), it is obvious from their work²¹ that the annealing induces a significant pileup.

IV. DISCUSSION

Now we return to the questions that we posed in the introduction and discuss the experimental results of this study in their context. In this study, the BMG samples experience free volume changes due to two reasons; one is due to the structural relaxation by sub- T_g annealing of the as-cast sample that leads to free volume reduction through annihilation, and the other is the increased free volume due to plastic deformation. While the former results in enhanced resistance to plastic flow, the latter results in flow softening. Spaepen⁵ suggested an equation for the amount of free volume created during deformation:

$$\Delta^+v = \frac{\gamma v^* 2kT}{v_f S} \left[\cosh\left(\frac{\tau\Omega}{2kT}\right) - 1 \right] Nv \times \exp\left(-\frac{\Delta G^m}{kT}\right) \exp\left(-\frac{\gamma v^*}{v_f}\right), \quad (2)$$

where γ is a geometric factor between 1 and 1/2, v^* is the atomic volume, v_f is the average free volume of an

atom, k is Boltzmann's constant, T is the absolute temperature, S is the elastic distortion energy, τ is the shear stress, Ω is the atomic volume, N is the total number of the atoms, v is the frequency, and ΔG^m is the activation energy of motion. In this equation, if v^*/v_f (which is always smaller than unity for an atom to be on a potential jump site) decreases, $(\gamma v^*/v_f) \times \exp(-\gamma v^*/v_f)$ gets algebraically smaller. As per this relation, relatively more free volume can be created during deformation in a sample that has a smaller initial free volume v_f to start with. In the present work, due to the reduction in free volume by annealing, the sample annealed for 90 min has the least amount of initial free volume among the three samples [see Fig. 2(b)]. Therefore, one might expect that the relative amount of the excess free volume during spherical indentation is the largest for the 90-min-annealed sample, which can result in more pronounced strain softening. However, the results obtained in the present work (Fig. 10) suggest that the degree of strain softening (i.e., the difference in relative hardness between the deformed region and the undeformed region) is almost independent of the initial free volume ($\sim 15.5\%$ for the as-cast sample and $\sim 12.5\%$ for the 90-min-annealed sample).

Very recently, Xie and George⁴⁵ analyzed the degree of strain softening measured by compression test on the as-cast and annealed BMG having the same composition as examined here. Calculations using the Vickers hardness data in Fig. 2(b) of their work⁴⁵ yield the relative hardness difference $[(H_{\text{undeformed}} - H_{\text{deformed}} \text{ (at strain} = 0.3\text{)}) / H_{\text{undeformed}}]$ of ~ 4.5 and $\sim 1\%$ for the as-cast sample and

the sample which was first deformed and then annealed at 633 K for 120 min, respectively. This small difference ($\sim 3.5\%$ between the as-cast and the annealed sample) also indicates that the extent of softening is not seriously affected by the initial free volume. The reason for the difference in decreasing amount between this work and the work of Xie and George⁴⁵ (i.e., for as-cast sample, $\sim 15.5\%$ versus $\sim 4.5\%$) might be related with different loading system, that is, the uniaxial stress state in compression versus the complex triaxial stress state in indentation. Also, the different range of applied plastic strain could conceivably be due to another reason. In the work of Xie and George,⁴⁵ the minimum plastic strain of the deformed sample is 0.3, which is much higher than that reached here during spherical indentation (of which the representative plastic strain is often estimated as $0.2a/R$ where a and R are the contact radius and the radius of the indenter tip)⁴⁹; for example, in the case of the as-cast sample, approximately 0.035 and 0.049 for $P_{\max} = 98$ N and 196 N, respectively. In their work,⁴⁵ no information was given for such a small plastic strain.

Another important question that we posed earlier is “does the number density of shear bands determine the extent of softening?” Observations made in this study imply that the flow stress of a metallic glass that has undergone plastic deformation is location independent, that is, the shear band has the same flow stress as that in between the bands. The fact that nanohardness data obtained at two different preloads (of 98 N and 196 N) fall on top of each supports the hypothesis. This is because the density of shear bands in these two cases is significantly different. If shear band number density were important, the plastic regime generated using the 196 N load should be relatively softer vis-à-vis that generated using the 98 N load, as the former has a higher number of bands. However, this was not the case. This observation led us to a possible answer to the above question, that is, the degree of softening is not seriously affected by the shear band density.

V. SUMMARY

In this study, the role of free volume in inhomogeneous plastic flow of the BMG was systematically analyzed by performing macroscopic spherical indentation and nanoindentation on the surface and subsurface of the as-cast and annealed samples. The primary results of this investigation are:

(1) The annealing treatment applied in this work did not induce crystallization but structural relaxation, and a large amount of free volume was annihilated during the structural relaxation process.

(2) While the structural relaxation annealing enhances hardness, both the subsurface shear band number density and the plastic zone size decrease with annealing time.

(3) The serrations in the nanoindentation load-displacement curves become smoother with structural relaxation, which could be analyzed with the discrete plasticity ratio in terms of the BMG's governing deformation mechanism.

(4) Regardless of the annealing condition, the nanoindentation hardness of the deformed regions is $\sim 12\text{--}15\%$ lower than the undeformed region, implying that the prior free volume only changes the yield stress (or hardness) but not the relative flow stress (or the extent of strain softening).

(5) Statistical distributions of the nanoindentation hardness obtained from deformed and undeformed regions have no overlap, suggesting that shear band number density has no influence on the plastic characteristics of the deformed region.

(6) AFM images obtained from the undeformed region exhibit a relatively larger amount of material pileup around the nanohardness impression than that from the deformed region. Also, for both the softened and the undeformed region, a larger amount of pileup is observed in the longer-annealed sample. Both phenomena could be analyzed in terms of free volume change and its role in plastic deformation.

Collectively, the important conclusion that can be drawn from this work is that the initial amount of free volume, while important in controlling plastic deformation (or strength/hardness) of BMGs, does not influence the extent of strain softening during deformation.

ACKNOWLEDGMENTS

This research was supported by the Korea Research Foundation (KRF) grant funded by the Korean Government, MEST (Grant No. KRF-2006-331-D00273), and partially by the Korea Science and Engineering Foundation (KOSEF) grant funded by MEST (Grant No. R01-2008-000-20778-0). One of the authors, U.R., acknowledges the financial support received for this work from the Department of Science and Technology, Government of India through a Swarna Jayanthi Fellowship. The authors thank Dr. H. Bei (at Oak Ridge National Laboratory) for providing the samples, and Mr. B-W. Choi (at Hanyang University) for his assistance in calculating the discrete plasticity ratio.

REFERENCES

1. C.A. Schuh, T.C. Hufnagel, and U. Ramamurty: Mechanical behavior of amorphous alloys. *Acta Mater.* **55**, 4067 (2007).

2. K.E. Prasad, R. Raghavan, and U. Ramamurty: Temperature dependence of pressure sensitivity in a metallic glass. *Scr. Mater.* **57**, 121 (2007).
3. M.N.M. Patnaik, R. Narasimhan, and U. Ramamurty: Spherical indentation response of metallic glasses. *Acta Mater.* **52**, 3335 (2007).
4. P. Tandaiya, R. Narasimhan, and U. Ramamurty: Mode I crack tip fields in amorphous materials with application to metallic glasses. *Acta Mater.* **55**, 6541 (2007).
5. F. Spaepen: A microscopic mechanism for steady state inhomogeneous flow in metallic glasses. *Acta Metall.* **25**, 407 (1977).
6. A.S. Argon: Plastic deformation in metallic glasses. *Acta Metall.* **27**, 47 (1979).
7. C.T. Liu, L. Heatherly, D.S. Easton, C.A. Carmichael, J.H. Schneibel, C.H. Chen, J.L. Wright, M.H. Yoo, J.A. Horton, and A. Inoue: Test environments and mechanical properties of Zr-base bulk amorphous alloys. *Metall. Mater. Trans. A* **29**, 1811 (1998).
8. M. Lind, G. Duan, and W.L. Johnson: Isoconfigurational elastic constants and liquid fragility of a bulk metallic glass forming alloy. *Phys. Rev. Lett.* **97**, 015501 (2006).
9. T. Egami: Formation and deformation of metallic glasses: Atomistic theory. *Intermetallics* **14**, 882 (2006).
10. K-W. Park, J-I. Jang, M. Wakeda, Y. Shibutani, and J-C. Lee: Atomic packing density and its influence on the properties of Cu-Zr amorphous alloys. *Scr. Mater.* **57**, 805 (2007).
11. C. Nagel, K. Ratzke, E. Schmidtke, J. Wolfe, U. Geyer, and F. Faupel: Free-volume changes in the bulk metallic glass $Zr_{46.7}Ti_{8.3}Cu_{7.5}Ni_{10}Be_{27.5}$ and the undercooled liquid. *Phys. Rev. B* **57**, 10224 (1998).
12. P. Tuinstra, P.A. Duine, J. Sietsma, and A. Vandenbeukel: The calorimetric glass-transition of amorphous $Pd_{40}Ni_{40}P_{20}$. *Acta Metall. Mater.* **43**, 2815 (1995).
13. O.P. Bobrov, V.A. Khonik, S.N. Laptev, and M.Y. Yazvitsky: Comparative internal friction study of bulk and ribbon glassy $Zr_{52.5}Ti_5Cu_{17.9}Ni_{14.6}Al_{10}$. *Scr. Mater.* **49**, 255 (2003).
14. A. Slipenyuk and J. Eckert: Correlation between enthalpy change and free volume reduction during structural relaxation of $Zr_{55}Cu_{30}Al_{10}Ni_5$ metallic glass. *Scr. Mater.* **50**, 39 (2004).
15. W. Dmowski, C. Fan, M.L. Morrison, P.K. Liaw, and T. Egami: Structural changes in bulk metallic glass after annealing below the glass-transition temperature. *Mater. Sci. Eng., A* **471**, 125 (2007).
16. U. Ramamurty, M.L. Lee, J. Basu, and Y. Li: Embrittlement of a bulk metallic glass due to low-temperature annealing. *Scr. Mater.* **47**, 107 (2002).
17. P. Murali and U. Ramamurty: Embrittlement of a bulk metallic glass due to sub- T_g annealing. *Acta Mater.* **53**, 1467 (2005).
18. R. Raghavan, P. Murali, and U. Ramamurty: Ductile to brittle transition in the $Zr_{41.2}Ti_{13.75}Cu_{12.5}Ni_{10}Be_{22.5}$ bulk metallic glass. *Intermetallics* **14**, 1051 (2006).
19. H.W. Jin, R. Ayer, J.Y. Koo, R. Raghavan, and U. Ramamurty: Reciprocating wear mechanisms in a Zr-based bulk metallic glass. *J. Mater. Res.* **22**, 264 (2007).
20. M.E. Launey, R. Busch, and J.J. Kruzic: Effects of free volume changes and residual stresses on the fatigue and fracture behavior of a Zr-Ti-Ni-Cu-Be bulk metallic glass. *Acta Mater.* **56**, 500 (2008).
21. W.H. Jiang, F.E. Pinkerton, and M. Atzmon: Mechanical behavior of shear bands and the effect of their relaxation in a rolled amorphous Al-based alloy. *Acta Mater.* **53**, 3469 (2005).
22. W.H. Wang, C. Dong, and C.H. Shek: Bulk metallic glasses. *Mater. Sci. Eng., R* **44**, 45 (2004).
23. A.R. Yavari, J.J. Lewandowski, and J. Eckert: Mechanical properties of bulk metallic glasses. *MRS Bull.* **32**, 635 (2007).
24. C.A. Schuh and T.G. Nieh: A survey of instrumented indentation studies on metallic glasses. *J. Mater. Res.* **19**, 46 (2004).
25. R. Bhowmick, R. Raghavan, K. Chattopadhyay, and U. Ramamurty: Plastic flow softening in a bulk metallic glass. *Acta Mater.* **54**, 4221 (2006).
26. U. Ramamurty, S. Jana, Y. Kawamura, and K. Chattopadhyay: Hardness and plastic deformation in a bulk metallic glass. *Acta Mater.* **53**, 705 (2005).
27. W.C. Oliver and G.M. Pharr: An improved technique for determining hardness and elastic modulus using load and displacement sensing indentation experiments. *J. Mater. Res.* **7**, 1564 (1992).
28. W.C. Oliver and G.M. Pharr: Measurement of hardness and elastic modulus by instrumented indentation: Advances in understanding and refinements to methodology. *J. Mater. Res.* **19**, 3 (2004).
29. D. Suh and R.H. Dauskardt: Flow and fracture in Zr-based bulk metallic glasses. *Ann. Chim.—Sci. Mat.* **27**, 25 (2002).
30. R. Bohmer, K.L. Ngai, C.A. Angell, and D.J. Plazek: Nonexperimental relaxations in strong and fragile glass formers. *J. Chem. Phys.* **99**, 4201 (1993).
31. R. Raghavan, P. Murali, and U. Ramamurty: Influence of cooling rate on the enthalpy relaxation and fragility of a metallic glass. *Metall. Mater. Trans. A* **39**, 1573 (2008).
32. K.L. Johnson: *Contact Mechanics*, 1st ed. (Cambridge University Press, Cambridge, UK, 1985).
33. C.A. Schuh and T.G. Nieh: A nanoindentation study of serrated flow in bulk metallic glasses. *Acta Mater.* **51**, 87 (2003).
34. W.H. Jiang and M. Atzmon: Rate dependence of serrated flow in a metallic glass. *J. Mater. Res.* **18**, 755 (2003).
35. A.L. Greer, A. Castellero, S.V. Madge, I.T. Walker, and J.R. Wilde: Nanoindentation studies of shear banding in fully amorphous and partially devitrified metallic alloys. *Mater. Sci. Eng., A* **375–377**, 1182 (2004).
36. C.A. Schuh, A.C. Lund, and T.G. Nieh: New regime of homogeneous flow in the deformation map of metallic glasses: Elevated temperature nanoindentation experiments and mechanistic modeling. *Acta Mater.* **52**, 5879 (2004).
37. B.C. Wei, L.C. Zhang, T.H. Zhang, D.M. Xing, J. Das, and J. Eckert: Strain rate dependence of plastic flow in Ce-based bulk metallic glass during nanoindentation. *J. Mater. Res.* **22**, 258 (2007).
38. B. Yang and T.G. Nieh: Effect of the nanoindentation rate on the shear band formation in an Au-based bulk metallic glass. *Acta Mater.* **55**, 295 (2007).
39. J-I. Jang, M.J. Lance, S. Wen, and G.M. Pharr: Evidence for nanoindentation-induced phase transformations in germanium. *Appl. Phys. Lett.* **86**, 131907 (2005).
40. J-I. Jang and G.M. Pharr: Influence of indenter angle on cracking in Si and Ge during nanoindentation. *Acta Mater.* **56**, 4458 (2008).
41. J-I. Jang, B-G. Yoo, and J-Y. Kim: Rate-dependent inhomogeneous-to-homogeneous transition of plastic flows during nanoindentation of bulk metallic glasses: Fact or artifact? *Appl. Phys. Lett.* **90**, 211906 (2007).
42. B-G. Yoo, J-Y. Kim, and J-I. Jang: Influence of indenter geometry on the deformation behavior of $Zr_{60}Cu_{30}Al_{10}$ bulk metallic glass during nanoindentation. *Mater. Trans.* **48**, 1765 (2007).
43. L. Wang, S.X. Song, and T.G. Nieh: Assessing plastic shear resistance of bulk metallic glasses under nanoindentation. *Appl. Phys. Lett.* **92**, 101925 (2008).
44. H. Bei, S. Xie, and E.P. George: Softening caused by profuse shear banding in a bulk metallic glass. *Phys. Rev. Lett.* **96**, 105503 (2006).
45. S. Xie and E.P. George: Hardness and shear band evolution in bulk metallic glasses after plastic deformation and annealing. *Acta Mater.* **56**, 5202 (2008).

46. B-G. Yoo and J-I. Jang: A study on the evolution of subsurface deformation in a Zr-based bulk metallic glass during spherical indentation. *J. Phys. D: Appl. Phys.* **41**, 074017 (2008).
47. C. Tang, Y. Li, and K. Zeng: Characterization of mechanical properties of a Zr-based metallic glass by indentation techniques. *Mater. Sci. Eng., A* **384**, 215 (2004).
48. W.H. Li, T.H. Zhang, D.M. Xing, B.C. Wei, Y.R. Wang, and Y.D. Dong: Instrumented indentation study of plastic deformation in bulk metallic glasses. *J. Mater. Res.* **21**, 75 (2006).
49. D. Tabor: *Hardness of Metals*, 1st ed. (Clarendon Press, Oxford, UK, 1951).